Structural basis for dual specificity of yeast N-terminal amidase in the N-end rule pathway

Min Kyung Kim[a], Sun Joo Oh[a], Byung-Gil Lee[a,1], and Hyun Kyu Song[a,2]

[a]Department of Life Sciences, Korea University, Seoul 02841, Korea

The first step of the hierarchically organized Arg/N-end rule pathway of protein degradation is deamidation of the N-terminal glutamine and asparagine residues of substrate proteins to glutamate and aspartate, respectively. These reactions are catalyzed by the N-terminal amidase (Nt-amidase) Nta1 in fungi such as *Saccharomyces cerevisiae*, and by the glutamine-specific Ntaq1 and asparagine-specific Ntan1 Nt-amidases in mammals. To investigate the dual specificity of yeast Nta1 (yNta1) and the importance of second-position residues in Asn/Gln-bearing N-terminal degradation signals (N-degrons), we determined crystal structures of yNta1 in the apo state and in complex with various N-degron peptides. Both an Asn-peptide and a Gln-peptide fit well into the hollow active site pocket of yNta1, with the catalytic triad located deeper inside the active site. Specific hydrogen bonds stabilize interactions between N-degron peptides and hydrophobic peripheral regions of the active site pocket. Key determinants for substrate recognition were identified and thereafter confirmed by using structure-based mutagenesis. We also measured affinities between yNta1 (wild-type and its mutants) and specific peptides, and determined K_M and k_{cat} for peptides of each type. Together, these results elucidate, in structural and mechanistic detail, specific deamidation mechanisms in the first step of the N-end rule pathway.

dual specificity | nitrilase superfamily | N-end rule | Nta1

The N-end rule pathway is a universally present ubiquitin (Ub)-dependent proteolytic system that mediates and regulates the degradation of intracellular proteins through the recognition of their (destabilizing) N-terminal residues (1–3). Some of the sterically exposed destabilizing N-terminal residues of N-end rule substrates are posttranslationally modified. The corresponding N-terminal degradation signals (N-degrons) are recognized by pathway's ubiquitin ligases, called N-recognins, which polyubiquitylate a substrate protein and, thereby, target it for the proteasome-mediated degradation (1, 4–6).

The N-end rule pathway has been demonstrated in all examined organisms, from prokaryotes (where it is independent of Ub) to multicellular eukaryotes, including animals and plants (7–10). Although details of pathway's organization can vary among remotely related organisms, the overall organization of the N-end rule pathway is largely the same in all species (11, 12). In eukaryotes, the tertiary destabilizing N-terminal residues Asn and Gln are deamidated, by specific N-terminal amidases (Nt-amidases), yielding N-terminal Asp and Glu, respectively. N-terminal Asp and Glu are arginylated by arginyl-tRNA transferase (arginyltransferase 1, encoded by *Ate1*), which conjugates Arg, a primary destabilizing residue, making it possible for N-recognins to recognize N-terminal Arg and target an N-end substrate for polyubiquitylation and degradation.

Eukaryotic N-recognins are Ubr-family E3 Ub ligases that recognize the primary destabilizing N-terminal residues Arg, Lys, His, Phe, Leu, Trp, Tyr, and Ile. Owing to the recent discovery of a separate, distinct branch of the N-end rule pathway that targets for degradation N-terminally acetylated (Nt-acetylated) N-terminal residues of cellular proteins (13–15), the above (initially discovered) branch was termed the Arg/N-end rule pathway, whereas the other branch was termed the Ac/N-end rule pathway.

Specificities of some enzymes in the Arg/N-end rule pathway are now partially understood through high-resolution structural studies (16–22). Interestingly, there is a marked difference in the first step of the Arg/N-end rule pathway between fungi on the one hand and animals and plants on the other hand. Specifically, in multicellular eukaryotes such as animals and plants, the first (Nt-deamidation) step is performed by two distinct enzymes, Ntan1 (it is specific for N-terminal Asn) and Ntaq1 (it is specific for N-terminal Gln). In contrast, the analogous deamidation of N-terminal Asn and Gln in fungal (including yeast) N-end rule substrates is mediated by a single enzyme, called Nta1 (23, 24).

Saccharomyces cerevisiae Nta1 (yNta1) was originally identified and cloned more than 20 y ago by the Varshavsky laboratory (23), which determined that yNta1 contains the catalytic triad Glu63–Lys136–Cys187 and that it deamidates sterically exposed N-terminal Asn or Gln but neither internal or C-terminal Asn or Gln residues. Despite the functional and historic significance of Nta1 (23), Nta1 enzymes from other fungal species remain largely uncharacterized. In addition, yNta1 belongs to the branch 3 of the nitrilase superfamily, which is classified into 13 branches according to substrate types. This family includes enzymes with the highly conserved Glu–Lys–Cys catalytic triad that hydrolyze nonpeptide carbon–nitrogen bonds (25). Although functional similarities have been identified among the mammalian Ntan1 and Ntaq1 versus yNta1, these Nt-amidases lack a significant sequelogy (sequence similarity) (26). In particular, save for the

Significance

The N-end rule pathway is a regulated protein degradation system. It is conserved among both prokaryotes and eukaryotes. In this hierarchically organized pathway, N-terminal amidase converts N-terminal Asn and N-terminal Gln, the tertiary destabilizing residues of N-end rule substrates, to the secondary destabilizing N-terminal residues Asp and Glu, respectively. The yeast (*Saccharomyces cerevisiae*) N-terminal amidase Nta1 was identified as a component of the N-end rule pathway more than 20 y ago, but its dual specificity for N-terminal Asn and Gln residues remains uncharacterized, owing the absence of structural and biochemical data. The present structures of yeast Nta1 with various N-degron peptides, and biochemical analyses with Nta1 mutants, illuminate specific mechanisms of the first step in the N-end rule pathway.
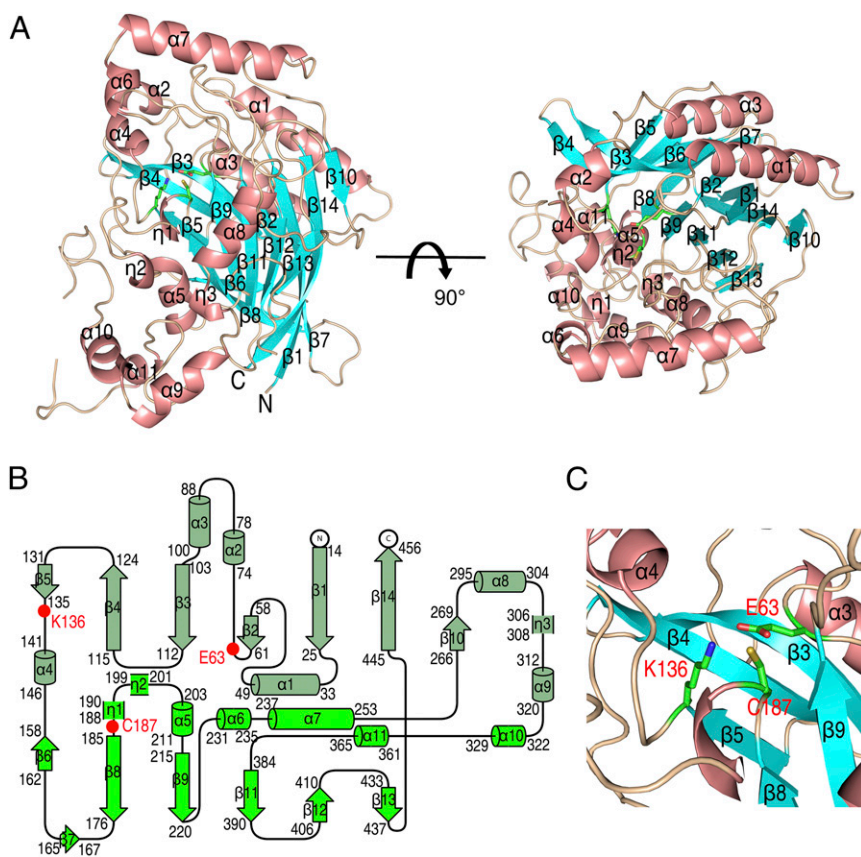
Fig. 1. Overall structure of *S. cerevisiae* Nta1. (*A, Left*) Ribbon diagram of yNta1. The α-helices and 3_{10}-helices, β-strands, and connecting loops are colored salmon, cyan, and wheat, respectively. (*A, Right*) View of a 90° rotation along the horizontal axis. (*B*) Topology diagram of yNta1. Catalytic residues (E63-K136-C187) are represented by red filled circles. (*C*) Close-up view of the active site. Cys187, Glu63, and Lys136 residues are shown as green sticks. Nitrogen, oxygen, and sulfur atoms are colored blue, red, and yellow, respectively.

common Cys residue, the active sites of the mammalian Ntan1 and Ntaq1 are dissimilar to that of yNta1 (22). Moreover, specific biological (as distinguished from mechanistic) functions of the Nt-amidases, including yNta1, remain poorly understood. Recent studies identified the mammalian Usp1 deubiquitylase as the first physiological substrate of Ntaq1 (22). In addition, deamidation assays with varied second residues of dipeptide substrate (27) confirmed that yNta1 does not deamidate-free Asn or Gln amino acids, that yNta1 is specific for dipeptides bearing N-terminal Asn or Gln, and that the second residue of a dipeptide influences the activity of yNta1 (27).

To investigate the dual specificity of yNta1 for N-terminal Asn and Gln of N-end rule substrates and to provide a structural foundation for future studies of Nt-deamidation, we determined the crystal structures of yNta1 in its apo-state and in complexes with substrates and their analogs. In addition, we determined the affinities (binding constants) of yNta1 to various substrate analogs and measured kinetic parameters such as K_M and k_{cat} for different kinds of peptide-based yNta1 substrates. We also carried out structure-based mutagenesis experiments with yNta1 that confirmed specific properties of this enzyme, thereby advancing the understanding of both the nitrilase family and the Arg/N-end rule pathway.

Results and Discussion

Overall Structure of yNta1. The *S. cerevisiae* Nt-amidase yNta1 contains Met residues at positions 1 and 11 (Fig. S1). The N-terminal sequence of yNta1 suggested the presence of a mitochondrial targeting sequence in this enzyme, and the possibility that the initiation of translation at two alternative Met residues might partition yNta1 in both the cytosol/nucleus and in mitochondria (23). Later evidence indicates that a significant fraction of yNta1 resides in the mitochondrial matrix (28). Therefore, two

Nta1 constructs [yNta1 (1) covering residues 1–457 and yNta1 (11) covering residues 11–457] were generated and analyzed. Both yNta1 (1) and yNta1 (11) were crystallized in the space groups $P4_2$ and $I4_122$, and their structures were determined at 2.32- and 2.7-Å resolution, respectively (Table S1). We could identify only 431 residues of 457 residues in yNta1 (1), because the N-terminal 12 residues and 2 loop regions (345–351 and 415–424) are not defined by the electron density. The overall structure has an α-β-β-α sandwich fold (Fig. 1*A* and Fig. S2), which is commonly found in members of the nitrilase superfamily (25, 29). In solution, yNta1 is a monomer (Fig. S3) containing 14 β-strands, 11 α-helices, and three 3_{10}-helices (Fig. 1*B* and Fig. S1). The core region of the enzyme shows antiparallel and parallel mixed β-sheets surrounded by helices, and these six-stranded β-sheets face each other (Fig. 1 *A* and *B*).

A previous study suggested that yNta1 comprises N-terminal hydrolase and C-terminal accessory domains (25). However, we observed no separate domains and stable globular folding. Moreover, the starting β-strand (β1) forms a β-sheet with the ending β-strand (β14) in antiparallel orientation, suggesting that N and C termini of yNta1 are close (Fig. 1*A*). The catalytic triad Cys187–Glu63–Lys136 is highly conserved among putative Nta1 enzymes from various organisms (Fig. S1), and the active site is located on a loop region that is distant from the N-terminal region (Fig. 1*C*), suggesting that N-terminal residues do not participate in the amidase activity. In agreement with these results, we found no differences in enzymatic activity between yNta1 (1) and yNta11 (11) constructs (Fig. S4). In addition, the catalytically inactive C187S mutant of yNta1 did not differ structurally from full-length wild-type yNta1. Consequently, structural studies of yNta1-containing complexes were performed with various peptide substrates and the yNta1 (11) C187S mutant (Table S2).
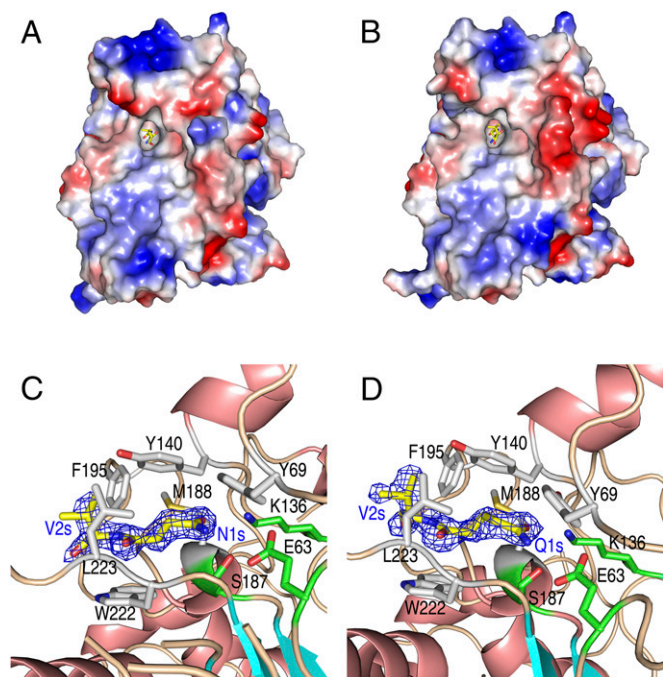
Fig. 2. Structures of N-degron–bound yNta1. Molecular surfaces are represented by electrostatic potential of yNta1 with Asn–Val (*A*) and with Gln–Val dipeptide (*B*). Negatively and positively charged surfaces are colored red and blue, respectively. N-degron peptides are shown as yellow sticks and are bound to the pocket of the active site of yNta1. Close-up view of N-degron binding site and electron-density map for the bound N-degrons Asn–Val (*C*) and Gln–Val dipeptide (*D*). The side chain atoms of catalytic and interacting residues of yNta1 are shown as green and gray stick models, respectively, and N-degron peptides are shown as yellow sticks. Oxygen and nitrogen atoms are colored red and blue, respectively. N-degron residues are labeled "s" after the residue number for clarity. Electron-density maps were generated and shown as blue mesh for each peptide (2*F*o-*F*c map contoured at 1.0 σ).

Interactions Between Nta1 and N-Degron Peptides. To further analyze functional properties of Nt-amidase, we solved yNta1 structures in complexes with six different N-degron peptides, including three Asn-dipeptides (NG, NV, NE), two Gln-dipeptides (QG, QV), and one Asn-tripeptide (NEA). The cleft of the active site could be tightly fitted to the Asn-peptide and Gln-peptide (Fig. 2 *A* and *B*), and no complex structures showed significant conformational changes, in comparison with the structures of free yNta1. Moreover, the binding modes with yNta1 differed only slightly for different peptide ligands (Fig. 2 *C* and *D* and Fig. S5). In particular, side chain amide groups of all N-degrons form hydrogen bonds with side chain atoms of the catalytic residues Lys136 and Ser187 (C187S mutant in structural studies). The carbonyl oxygen atom of the main chain of Ala221 forms a hydrogen bond with the nitrogen atoms of amide groups of N-degrons, except for those of Gln–Gly and Asn–Glu–Ala peptides (Fig. S6). The nitrogen atom of Leu223 forms a hydrogen bond with the carbonyl oxygen atom of N-terminal Asn or Gln of peptide substrates. These residues of yNta1 contact N-terminal Asn and Gln over significant fractions of their length. N-terminal Asn/Gln-bearing N-degrons are also surrounded by a hydrophobic pocket comprising Tyr69, Tyr140, Met188, Phe195, Trp222, and Leu223 of yNta1 (Fig. 2 and Fig. S5). In particular, the tyrosine residues Tyr140 and Tyr69 are located in the upper region, in the orientation shown in Fig. 2, and the bulky Trp222 residue is located in the lower region of the hydrophobic pocket. Met188, Phe195, and Leu223 residues of yNta1 are located at both sides of the pocket (Fig. 2 and Fig. S5), but appear less important for the binding to N-degron peptides

than the above-mentioned hydrogen bonds, which are critical for the affinity of Nta1 for the N-terminal Asn/Gln-bearing N-degrons.

Gln residues have longer side chains than Asn residues, differing by one methylene group. Thus, the Gln-peptide may reach slightly deeper into the active site. Interestingly, the hydrogen bonds are formed with all three catalytic triad residues in the case of Gln-peptide, whereas the Asn-peptide does not interact with Glu63 (Fig. S6). Moreover, residues of the active site of yNta1 did not show high structural plasticity in that the atomic positions of the N-degron recognizing residues differed little between the yNta1 complexes with either the Asn-peptide or the Gln-peptide (Fig. 3*A*). Instead, to fit into the rigid active site, the side chain of the Gln-peptide is not extended as much as is the side chain of the Asn-peptide (Fig. 3*A*). In addition, the residue of the Gln-peptide at position 2 made a specific contact with Phe195 of yNta1. These results suggest that the active site of yNta1 is best fitted vis-à-vis the recognition of N-terminal Asn-bearing N-degrons, and that more residues of yNta1 are required to accommodate the N-terminal Gln-bearing N-degron.
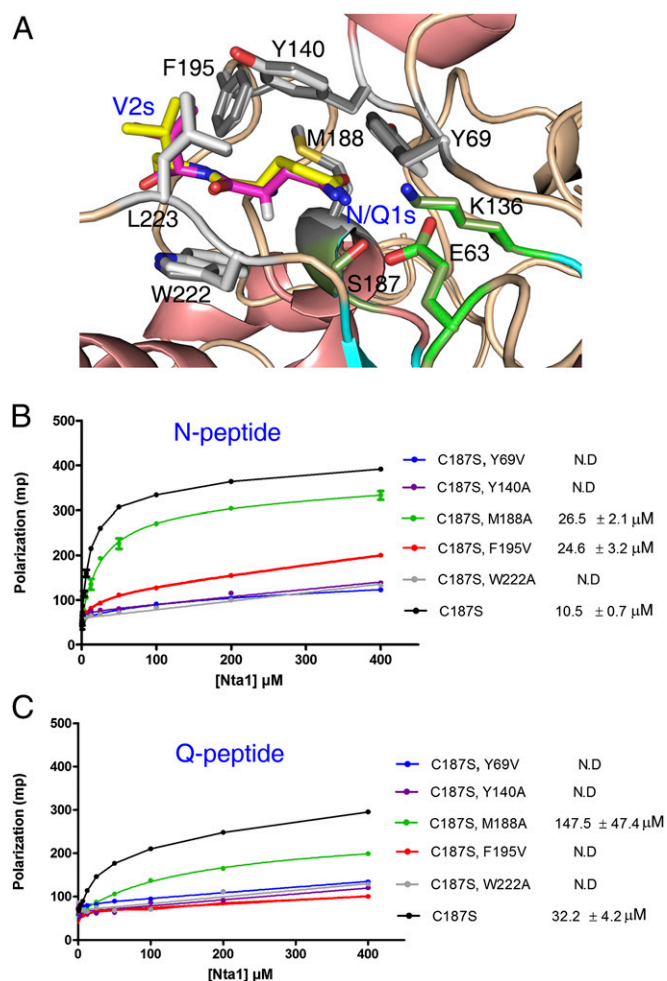

Fig. 3. N-degron binding affinity and effects of hydrophobic residues of yNta1. (*A*) Superposition of N- and Q-peptide–bound yNta1 structures. Side chain atoms of Gln-peptide–bound yNta1 are dark colored, and their positions are virtually identical. Bound Asn- and Gln-peptides are colored magenta and yellow, respectively. (*B*) Binding affinity measurements using C-terminal FITC-labeled NVK-peptide against increasing concentrations of yNta1 mutants (Y69V, Y140A, M188A, F195V, and W222A). (*C*) FP assays using C-terminal FITC-labeled QVK-peptide against increasing concentrations of yNta1 mutants; K_D values were calculated from at least three independent experiments; N.D, not determined.
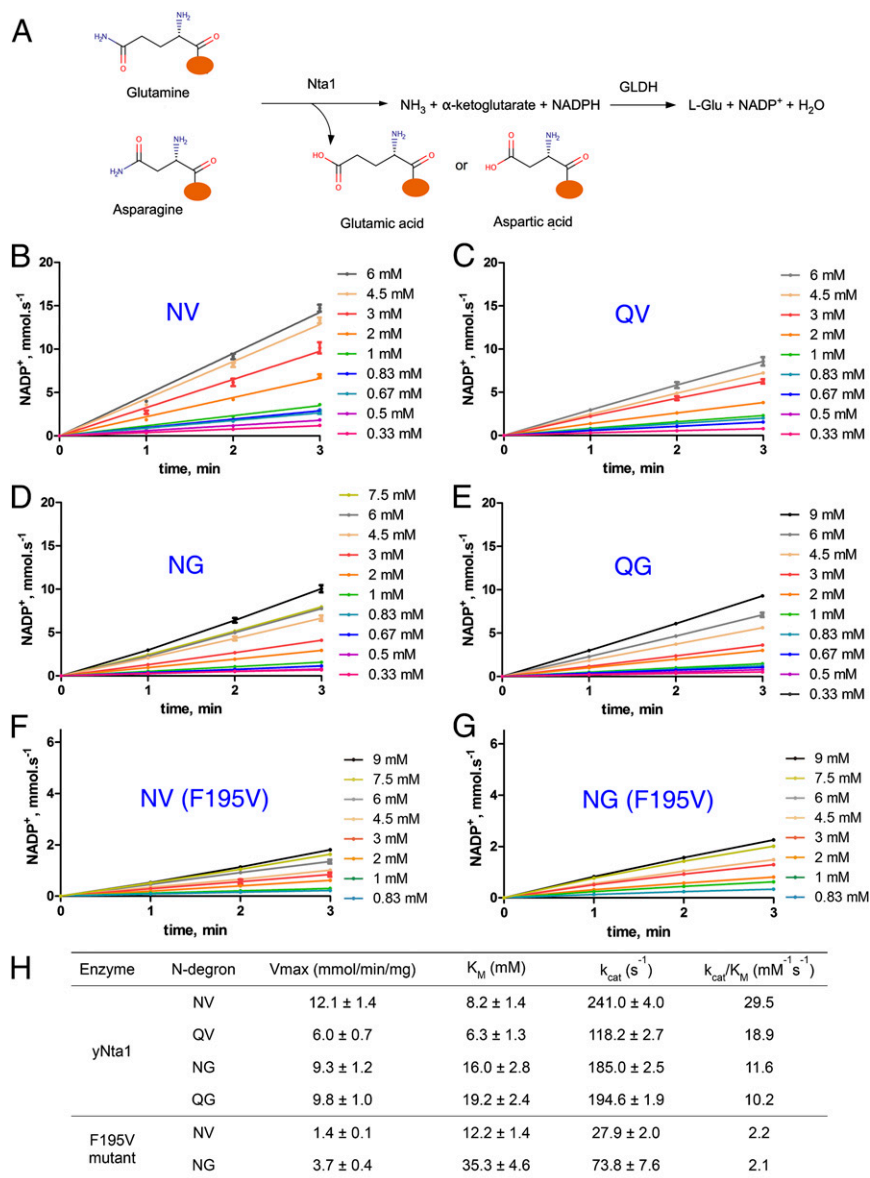
Fig. 4. N-terminal amidase activities. (A) Scheme for coupled enzymatic assays. Deamidation of N-terminal Asn or Gln was measured according toreleased ammonia (NH_3) by using NADPH-dependent GLDH. NH_3-dependent conversion of NADPH to $NADP^+$ by GLDH was monitored by using a spectrophotometer. GLDH coupled enzyme kinetics of purified wild-type yNta1 with the dipeptides NV (B), QV (C), NG (D), and QG (E), and that of F195V mutant with the dipeptides NV (F) and NG (G). Rates of $NADP^+$ formation were linear and only depended on concentrations of dipeptide at the indicated times. Standard derivations for triplicate measurements are indicated with error bars. (H) Summary of kinetic parameters of wild-type and a mutant yNta1 with various N-degron substrates.

Enzyme	N-degron	Vmax (mmol/min/mg)	K_M (mM)	k_{cat} (s^{-1})	k_{cat}/K_M ($mM^{-1} s^{-1}$)
yNta1	NV	12.1 ± 1.4	8.2 ± 1.4	241.0 ± 4.0	29.5
	QV	6.0 ± 0.7	6.3 ± 1.3	118.2 ± 2.7	18.9
	NG	9.3 ± 1.2	16.0 ± 2.8	185.0 ± 2.5	11.6
	QG	9.8 ± 1.0	19.2 ± 2.4	194.6 ± 1.9	10.2
F195V mutant	NV	1.4 ± 0.1	12.2 ± 1.4	27.9 ± 2.0	2.2
	NG	3.7 ± 0.4	35.3 ± 4.6	73.8 ± 7.6	2.1

In our further analyses, we determined the structures of yNta1 complexes with the Asn-peptide containing three different residues at the second position, including the hydrophobic Val, the side chain-lacking Gly, and the acidic Glu (Table S2). In contrast with Asn-Val and Asn-Gly dipeptides, the carboxylic group of Glu2 in the Asn-Glu dipeptide forms a hydrogen bond with the hydroxyl group of Tyr140, and the Asn-Glu dipeptide forms additional hydrophobic interactions with Thr229 (Fig. S6 E and F). In addition, the Asn-Glu-Ala tripeptide forms additional hydrophobic interactions with Tyr300, although the contribution of this interaction appears to be minor.

Binding of N-Terminal Asn/Gln-Bearing Peptides to yNta1. As described above, the catalytically important residues of yNta1 form hydrogen bonds with N-terminal Asn/Gln-bearing N-degrons obviously, and main chain atoms of the residues Ala221 and Leu223 form hydrogen bonds that could not be examined further in mutagenesis experiments. Because the hydrophobic binding pocket of Nta1 is formed by side chain atoms of its critical residues, we mutated several of these residues and directly measured the binding between the resulting mutants and N-degron peptides.

Because the C-terminal region of an N-degron, in a tripeptide, was not recognized by yNta1, it allowed the conjugation of fluorescent FITC to the C terminus of NVK and QVK tripeptides, followed by determination of dissociation constants (K_D), using fluorescence polarization (FP) with the corresponding yNta1 complexes. In initial FP experiments with wild-type yNta1, the data were variable, most likely owing to deamidation activity of yNta1. Subsequent experiments were used, therefore, with specific C187S-based mutants of yNta1 that lacked Nt-amidase activity. Before introducing specific mutations, we determined the binding affinity of yNta1 (C187S) for NVK-FITC and QVK-FITC peptides (Fig. 3 B and C). These analyses showed that the affinity of yNta1 for the N-terminal Asn-bearing N-degron is ~threefold higher than that for the otherwise identical N-terminal Gln-bearing N-degron peptide. Owing to this weaker binding, crystals of Gln-peptide bound to yNta1 were initially difficult to generate. In addition, the second Gly residue in the Gln-Gly (QG) dipeptide was not visible in the electron-density map (Fig. S5B).

On the basis of the present complex structures, we generated yNta1 mutant in which side chains of a nonpolar residue or aromatic residues are mutated (M188A, Y69V, Y140A, F195V,
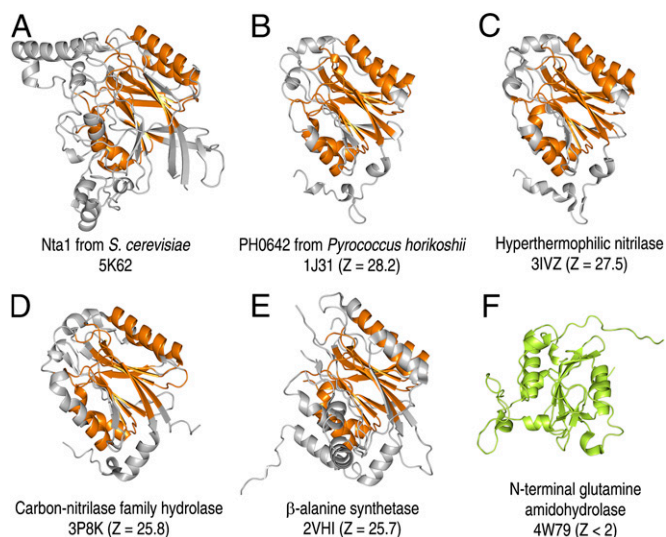
Fig. 5. Comparison of the overall structures of yNta1 with other spalogs (26). Ribbon diagrams comparing overall structures of yNta1 (*A*), PH0642, putative CN hydrolase from *Pyrococcus horikoshii* (*B*), hyperthermophilic nitrilase (*C*), putative carbon-nitrogen family hydrolase from *Staphylococcus aureus* (*D*), β-alanine synthetase (*E*), and N-terminal glutamine amidohydrolase (*F*). To clarify the region, the presented view represents approximately −20° and 50° horizontal and vertical rotations, respectively, of the images in Fig. 1*A*. Structural regions that match the corresponding region of yNta are colored orange in each structure. Structurally dissimilar (Z score below 2) N-terminal glutamine amidohydrolase in *F* is colored green. PDB ID codes and Z scores from the DALI server are shown below each structure.

and W222A) in the background of the inactive C187S mutant. The M188A mutant, which has a shortened aliphatic side chain at position 188, had 2.5-fold and 4.6-fold lower binding affinity for the Asn-peptide and Gln-peptide, respectively, suggesting that this alteration was more sensitive to the binding of Gln-peptide. All aromatic side chain mutations in yNta1 abolished the binding to the Gln-peptide (Fig. 3*C*) and all but F195V failed to bind the Asn-peptide, whereas the F195V mutant bound this peptide with a 2.5-fold reduction in affinity (Fig. 3*B*). These results confirm the importance of the relevant hydrophobic residues of yNta1 for substrate recognition. In addition, the F195V mutant bound the NVK-peptide with K_D of 24.6 μM, but did not bind the QVK-peptide, suggesting that the Phe195 of yNta1 plays a more important role in the binding to the Gln-peptide than in the binding to the Asn-peptide. As mentioned above, the Phe195 residue interacts with the second residue of an N-terminal Asn/Gln-bearing N-degron. In contrast with the Asn-peptide, the side chain of N-terminal Gln was slightly distorted to fit into the active site. These observations indicate that the side chains of N-degrons' second residues move outward to the Phe195 ring position (Fig. 3*A*). Accordingly, the less bulky side chain at position 195 in the F195V mutant caused more severe binding defects vis-à-vis the Gln-peptide (Fig. 3*C*).

N-Terminal Deamidation Activity of yNta1. In addition to measuring binding affinities of yNta1 for the Asn-peptides and Gln-peptides, we also determined the dual Nt-amidase activities by using the dipeptides NG, QG, NV, and QV. We also determined the structures of yNta1 in the presence of these peptides and those with the Glu residue position 2 (Fig. 2 and Fig. S5). The Nt-amidase activity assays with Asn–Glu and Gln–Glu dipeptides peptides were not feasible, owing to the use of the coupled NADPH-dependent glutamate dehydrogenase (GLDH) reaction, because GLDH also recognizes Glu at the second position and dehydrogenates it rapidly (Fig. 4*A*). Consequently, the production of

ammonia (NH_3) from amide groups of Asn and Gln by yNta1 was measured with technically feasible substrates using the GLDH enzyme, which converts NADPH, ammonia, and α-ketoglutarate to water, L-Glu, and $NADP^+$. Purified wild-type yNta1 and F195V mutants that bind the Asn-peptide were used to analyze the enzyme kinetics (Fig. 4 *B–G*). We observed no differences in the Nt-amidase activity between yNta1 (1) and yNta1 (11) (Fig. S4). Consequently, the subsequent binding affinity measurements, activity assays, and structural studies were performed with yNta1 (11), which could be overproduced more readily than yNta1 (1).

The yNta1 Nt-amidase requires similar concentrations of Asn-peptides and Gln-peptide substrates for saturation, as indicated by similar K_M values with the same second-residue position but differing N-terminal residues, Asn versus Gln (see K_M values for NV vs. QV and NG vs. QG in Fig. 4*H*). In addition, yNta1 exhibits similar catalytic rates (k_{cat}) with both NG and QG peptides, and approximately twice that rate with Asn-Val, in which position 2 is occupied by Val. These results indicate a slight preference of yNta1 for the hydrophobic residue at the second position of an N-terminal Asn/Gln-bearing N-degron. It should be noted that the Nt-deamidation activity of yNta1 was influenced by the identity of a residue at position 2 more than by N-terminal Asn and Gln. Moreover, the measured relative substrate specificities (k_{cat}/K_M) clearly show that yNta1 prefers the Asn-peptide with a hydrophobic residue at position 2 (Fig. 4*H*). The F195V mutant of yNta1 only exhibited a significant binding for the Asn-peptide but not the Gln-peptide (Fig. 3*B*). There was, in addition, a major decrease in enzyme specificity, mainly due to the lowered k_{cat}, compared with wild-type yNta1. However, the specificities for NV and NG peptides were nearly compensated by K_M and k_{cat} values (Fig. 4*H*). These data show that effects of the residue at position 2 might be more critical in Gln-peptide than Asn-peptide.

Given our binding affinity and enzyme kinetics data (Figs. 3 and 4), the dual specificity of yNta1 reflects the presence of an optimized binding pocket that recognizes both the Asn-peptide and Gln-peptide, with the longer side chain of Gln being slightly distorted to fit into the active site. Accordingly, hydrogen bonds with the catalytic residues Glu63, Lys136, and Cys187 are primary specificity determinants for N-terminal Asn/Gln-bearing N-end rule substrates. In addition, two hydrogen bonds from main chain atoms (Ala221 and Leu223) contribute to the binding affinity but not the enzymatic specificity for both the Asn-peptide and Gln-peptide. Finally, the surrounding hydrophobic interactions of Tyr69, Tyr140, Met188, Phe195, and Trp222 residues are partially involved in both substrate binding and product release, with some structural plasticity vis-à-vis the second residue of an N-degron (Fig. S6).

Comparisons with Human Ntaq1. Previous studies of the Arg/N-end rule pathway in yeast and mammals have shown that substantially different Nt-amidases deamidate N-terminal Asn and Gln in different organisms. Specifically, whereas *S. cerevisiae* Nta1 (yNta1) deamidates both N-terminal Asn and Gln, to separate mammalian Nt-amidases, Ntan1 and Ntaq1, deamidate N-terminal Asn and Gln, respectively (11). Remarkably, despite the closely similar Nt-deamidation reactions catalyzed by these Nt-amidases, yNta1 is essentially nonsequelogous (26) to either human Ntan1 or human Ntaq1 (8% and 11% sequence identity, respectively). Moreover, human Ntaq1 (hNtaq1) is structurally and mechanistically similar to transglutaminase (22), whereas yNta1 is a member of the nitrilase superfamily. Comparisons with other known structures using the DALI server (30) showed high structural similarities (Z score > 25) with the putative CN hydrolase protein PH0642 (PDB ID code 1J31) (31), a hyperthermophilic nitrilase (PDB ID code 3IVZ) (29), a putative carbon–nitrogen family hydrolase from *S. aureus* (PDB ID code 3P8K), and a β-alanine synthetase (PDB ID code 2VHI) (32)

(Fig. 5). In particular, the central β-sheet is almost identical in all of these structures, and yNta1 has a C-terminal region additional to those of the previously solved nitrilase superfamily proteins (Fig. 5C). However, in contrast to yNta1, nitrilase family proteins contain C-terminal motifs that mediate the formation of oligomers. For example, PH0642, hyperthermophilic nitrilase, and the putative carbon–nitrogen family hydrolase are dimers, and β-alanine synthetase is a helical octamer with tightly packed dimeric units. A C-terminal region of yNta1 that is absent from other nitrilases comprises a long disordered loop region containing helices (Fig. 5A) that ensures that yNta1 exists as a monomer in solution (Fig. S3).

As would be expected from the negligible sequelogy (sequence similarity) to yNta1 and the more restricted Nt-deamidation activity, the overall structure of hNtaq1 differs greatly from that of yNta1 (Fig. 5F). The structure of human Ntan1 has not been determined yet. The initially deposited structure of hNtaq1 (PDB ID code 3C9Q) was misinterpreted vis-a-vis the electron density of a bound peptide. Later refinements (PDB ID code 4W79) identified the "peptide" as an N-terminal region of the neighboring hNtaq1 molecule in the crystalline lattice, bearing the sequence Ser–Glu–Gly–, i.e., this sequence is not an actual substrate of hNtaq1 (21). In addition, hNtaq1 carries different catalytic triad residues (Cys28–His81–Asp97) that form a different spatial orientation, in comparison with the Glu63–Lys136–Cys187 catalytic triad of yNta1 (Fig. S7). The residues of the catalytic triad in hNtaq1 are not involved in direct contacts with cognate Nt-deamidation substrates as shown in yNta1 (Fig. 2 C and D). Moreover, the "recognition" residues of hNtaq1 are entirely distinct from those of yNta1. In yet another contrast with yNta1, two water molecules are proposed to be involved in the catalytic cycle of hNtaq1 (21). The enzymatic mechanism of yNta1 is essentially similar to that of N-carbamyl-D-amino acid amidohydrolase (33) (Fig. S8).

Apart from the structural and biological significance of our results about yNta1, its dual specificity for N-terminal Asn/Gln-bearing peptides may be exploited in industrial applications, such as production of the artificial sweetener aspartame (Asp-Phe-OMe, L-aspartyl-L-phenylalanine-methyl ester) (27). In contrast to mammalian Nt-amidases, no physiological substrate of yNta1 N-terminal amidase has been identified in yeast so far. The biological significance of a partially mitochondrial location of yNta1 remains to be understood as well. Our structural and substrate-binding data about yNta1 should be helpful in further studies of this conserved component of the Arg/N-end rule pathway.

Materials and Methods

Details on protein expression, purification, crystallization, structure determination, biochemical assays, and binding constant measurements are provided in *SI Materials and Methods*.

1. Bachmair A, Finley D, Varshavsky A (1986) In vivo half-life of a protein is a function of its amino-terminal residue. *Science* 234(4773):179–186.
2. Gonda DK, et al. (1989) Universality and structure of the N-end rule. *J Biol Chem* 264(28):16700–16712.
3. Varshavsky A (1992) The N-end rule. *Cell* 69(5):725–735.
4. Varshavsky A (1996) The N-end rule: Functions, mysteries, uses. *Proc Natl Acad Sci USA* 93(22):12142–12149.
5. Bartel B, Wünning I, Varshavsky A (1990) The recognition component of the N-end rule pathway. *EMBO J* 9(10):3179–3189.
6. Mogk A, Schmidt R, Bukau B (2007) The N-end rule pathway for regulated proteolysis: Prokaryotic and eukaryotic strategies. *Trends Cell Biol* 17(4):165–172.
7. Tobias JW, Shrader TE, Rocap G, Varshavsky A (1991) The N-end rule in bacteria. *Science* 254(5036):1374–1377.
8. Shrader TE, Tobias JW, Varshavsky A (1993) The N-end rule in Escherichia coli: Cloning and analysis of the leucyl, phenylalanyl-tRNA-protein transferase gene aat. *J Bacteriol* 175(14):4364–4374.
9. Potuschak T, et al. (1998) PRT1 of Arabidopsis thaliana encodes a component of the plant N-end rule pathway. *Proc Natl Acad Sci USA* 95(14):7904–7908.
10. Dougan DA, Truscott KN, Zeth K (2010) The bacterial N-end rule pathway: Expect the unexpected. *Mol Microbiol* 76(3):545–558.
11. Varshavsky A (2011) The N-end rule pathway and regulation by proteolysis. *Protein Sci* 20(8):1298–1345.
12. Tasaki T, Sriram SM, Park KS, Kwon YT (2012) The N-end rule pathway. *Annu Rev Biochem* 81:261–289.
13. Hwang CS, Shemorry A, Auerbach D, Varshavsky A (2010) The N-end rule pathway is mediated by a complex of the RING-type Ubr1 and HECT-type Ufd4 ubiquitin ligases. *Nat Cell Biol* 12(12):1177–1185.
14. Shemorry A, Hwang CS, Varshavsky A (2013) Control of protein quality and stoichiometries by N-terminal acetylation and the N-end rule pathway. *Mol Cell* 50(4):540–551.
15. Park SE, et al. (2015) Control of mammalian G protein signaling by N-terminal acetylation and the N-end rule pathway. *Science* 347(6227):1249–1252.
16. Choi WS, et al. (2010) Structural basis for the recognition of N-end rule substrates by the UBR box of ubiquitin ligases. *Nat Struct Mol Biol* 17(10):1175–1181.
17. Matta-Camacho E, Kozlov G, Li FF, Gehring K (2010) Structural basis of substrate recognition and specificity in the N-end rule pathway. *Nat Struct Mol Biol* 17(10):1182–1187.
18. AhYoung AP, Koehl A, Vizcarra CL, Cascio D, Egea PF (2016) Structure of a putative ClpS N-end rule adaptor protein from the malaria pathogen Plasmodium falciparum. *Protein Sci* 25(3):689–701.
19. Román-Hernández G, Grant RA, Sauer RT, Baker TA (2009) Molecular basis of substrate selection by the N-end rule adaptor protein ClpS. *Proc Natl Acad Sci USA* 106(22):8888–8893.
20. Schuenemann VJ, et al. (2009) Structural basis of N-end rule substrate recognition in Escherichia coli by the ClpAP adaptor protein ClpS. *EMBO Rep* 10(5):508–514.
21. Park MS, et al. (2014) Crystal structure of human protein N-terminal glutamine amidohydrolase, an initial component of the N-end rule pathway. *PLoS One* 9(10):e111142.
22. Wang H, Piatkov KI, Brower CS, Varshavsky A (2009) Glutamine-specific N-terminal amidase, a component of the N-end rule pathway. *Mol Cell* 34(6):686–695.
23. Baker RT, Varshavsky A (1995) Yeast N-terminal amidase. A new enzyme and component of the N-end rule pathway. *J Biol Chem* 270(20):12065–12074.
24. Grigoryev S, et al. (1996) A mouse amidase specific for N-terminal asparagine. The gene, the enzyme, and their function in the N-end rule pathway. *J Biol Chem* 271(45):28521–28532.
25. Pace HC, Brenner C (2001) The nitrilase superfamily: Classification, structure and function. *Genome Biol* 2(2):reviews0001.1–reviews0001.9.
26. Varshavsky A (2004) 'Spalog' and 'sequelog': Neutral terms for spatial and sequence similarity. *Curr Biol* 14(5):R181–R183.
27. Arai T, Noguchi A, Takano E, Kino K (2013) Application of protein N-terminal amidase in enzymatic synthesis of dipeptides containing acidic amino acids specifically at the N-terminus. *J Biosci Bioeng* 115(4):382–387.
28. Huh WK, et al. (2003) Global analysis of protein localization in budding yeast. *Nature* 425(6959):686–691.
29. Raczynska JE, Vorgias CE, Antranikian G, Rypniewski W (2011) Crystallographic analysis of a thermoactive nitrilase. *J Struct Biol* 173(2):294–302.
30. Holm L, Rosenstrom P (2010) Dali server: Conservation mapping in 3D. *Nucleic Acids Res* 38(Web Server issue):W545–549.
31. Sakai N, Tajika Y, Yao M, Watanabe N, Tanaka I (2004) Crystal structure of hypothetical protein PH0642 from Pyrococcus horikoshii at 1.6A resolution. *Proteins* 57(4):869–873.
32. Lundgren S, Lohkamp B, Andersen B, Piskur J, Dobritzsch D (2008) The crystal structure of beta-alanine synthase from Drosophila melanogaster reveals a homooctameric helical turn-like assembly. *J Mol Biol* 377(5):1544–1559.
33. Nakai T, et al. (2000) Crystal structure of N-carbamyl-D-amino acid amidohydrolase with a novel catalytic framework common to amidohydrolases. *Structure* 8(7):729–737.
34. Lee BG, Kim MK, Kim BW, Suh SW, Song HK (2012) Structures of the ribosome-inactivating protein from barley seeds reveal a unique activation mechanism. *Acta Crystallogr D Biol Crystallogr* 68(Pt 11):1488–1500.
35. Minor W, Tomchick D, Otwinowski Z (2000) Strategies for macromolecular synchrotron crystallography. *Structure* 8(5):R105–R110.
36. Adams PD, et al. (2010) PHENIX: A comprehensive Python-based system for macromolecular structure solution. *Acta Crystallogr D Biol Crystallogr* 66(Pt 2):213–221.
37. McCoy AJ, et al. (2007) Phaser crystallographic software. *J Appl Cryst* 40(Pt 4):658–674.
38. Emsley P, Cowtan K (2004) Coot: Model-building tools for molecular graphics. *Acta Crystallogr D Biol Crystallogr* 60(Pt 12 Pt 1):2126–2132.

BIOCHEMISTRY

Supporting Information

Kim et al. 10.1073/pnas.1612620113

SI Materials and Methods

Protein Expression and Purification. The *yNta1* gene was amplified by using PCR with *S. cerevisiae* genomic DNA. PCR products were cloned into the pET-RIP plasmid, which is a modified pET vector containing a N-terminal 6×His-bRIP (ribosome inactivation protein from barley) tagged protein followed by a TEV protease cleavage site (34). Subsequently, yNta1 was expressed in *Escherichia coli* BL21(DE3) cells in LB media, and the cells were induced at an OD of 0.6 following the addition of 1 mM isopropyl-β-D-thiogalactopyranoside (IPTG) and were cultured at 18 °C for 18 h. Cells were harvested by centrifugation and were resuspended in buffer A [50 mM Tris·HCl pH 8.0, 100 mM NaCl, and 2 mM tris(2-carboxyethyl)phosphine (TCEP)] and were then disrupted by sonication. Cell debris was removed by centrifugation and supernatants were loaded onto Ni-NTA columns (GE Healthcare) and eluted with gradually increasing concentrations of imidazole (30–500 mM). N-terminal bRIP-tags were then removed by overnight incubation with TEV protease, and remaining constructs were further purified by using Q-Sepharose anion exchange column (GE Healthcare). To remove remaining the bRIP tag, construct samples were added to Ni-NTA columns (GE Healthcare) and were finally purified by using Superdex 75 gel filtration columns (GE Healthcare) eluted with buffer A. Selenomethionyl derivatized yNta1 was expressed by using the methionine auxotrophic *E. coli* B834 strain in M9 media. Various mutant proteins were generated by using QuikChange mutagenesis kits, and selenomethionyl and mutant proteins were purified by using the same procedure.

Crystallization, Data Collection, and Structural Determination. Purified proteins were concentrated to 5 mg/mL for crystallization screening. Crystallization of yNta1 was achieved by mixing 1 μL of protein solution with the same volume of crystallization solution followed by equilibriation against 120~200 μL of a reservoir at 20 °C by using a hanging drop vapor diffusion method. Crystals were grown within 2 d. To cocrystallize purified yNta1, C187S mutant was incubated with ~25-fold molar excesses of each peptide for 24 h and was then subjected to the following optimized crystallization conditions for each protein: yNta1, 0.2 M ammonium acetate, 0.1 M tri-Na-citrate dihydrate pH 5.6 and 30% (wt/vol) PEG 4000; yNta11 and yNta11 C187S mutant, 0.2 M Mg-acetate tetrahydrate, 0.2 M Na-cacodylate pH 6.5, and 20% (wt/vol) PEG 8000; selenomethionyl-labeled yNta11 M196L, 0.2 M ammonium sulfate, 0.1 M Tris·HCl pH 8.8, and 24% (wt/vol) PEG 3350.

Because initial SeMet crystals of yNta1 or yNta11 did not diffract well, we generated the three mutants M11L, M196L, and M333L to decrease numbers of selenium substitutions. Among these mutants, the yNta11 M196L mutant successfully produced SeMet crystals that diffract to 2.3 Å under the above crystallization conditions. To phase this selenomethionyl-substituted yNta11 M196L crystal, three-wavelength multiwavelength anomalous diffraction datasets were collected at the absorption edge and peak of the Se atom, and at a high-energy wavelength (Table S1). Diffraction data were collected at the beamline 5C Pohang accelerator laboratory (Pohang, Korea) and at the beamline NE3A Photon Factory (Tsukuba, Japan), and the datasets were integrated and scaled by using the HKL2000 software package (35). The structure

of yNta11 was solved by using Autosol according to the PHENIX software suite (36), and was refined by using the program PHENIX. Structures of yNta11 C187S and its complex with six different substrate peptides were determined by using the molecular replacement method with PHASER (37). The model was then rebuilt with the program COOT (38) and was refined by using PHENIX. The DALI server (ekhidna.biocenter.helsinki.fi/dali_server/) was used to compare structures (30), and all structural figures were drawn by using PyMOL (www.pymol.org/).

Deamidation Activity Assays. Deamidation of peptides containing N-terminal Asn and Gln was determined by quantifying the production of ammonia (NH_3) in the presence of NADPH-dependent glutamate dehydrogenase. Consumption of NADPH was measured according to decreases in A_{340}, allowing indirect assay of Nt-amidase activity (Fig. 4A). Specifically, either free glutamine or synthetic peptides (NV, NG, QV, and QG dipeptide) were preincubated with 0.5 M NADPH, 7.6 mM oxoglutarate, and 4 units of glutamate dehydrogenase in buffer containing 50 mM Tris·HCl (pH 8.0) and 100 mM NaCl at 37 °C for approximately 10 min until A_{340} became stable. The reaction was initiated by the addition of various concentrations of substrate peptide (1.17 μL) to the final reaction mixture, which had a total volume of 65 μL. The rate of ammonia formation was measured according to increases in A_{340} for 30 min at 37 °C. Measurements were performed in triplicate, and data were analyzed by using GraphPad Prism 5 (GraphPad Software).

Size-Exclusion Chromatography with Multiangle Light Scattering. Size-exclusion chromatography with multiangle light scattering (SEC–MALS) experiments were performed by using a fast protein liquid chromatography system (GE Healthcare) connected to a Wyatt MiniDAWN TREOS MALS instrument and a Wyatt Optilab rEX differential refractometer. A Superdex 75 10/300 GL (GE Healthcare) gel filtration column preequilibrated with 50 mM Tris·HCl pH 8.0, 100 mM NaCl, and 1 mM TCEP was normalized by using chicken egg white lysozyme protein. Complexed or individual uncomplexed proteins were prepared as described earlier and were injected (1–3 mg/mL, 0.5 mL) at a flow rate of 0.5 mL/min. Data were analyzed by using the Zimm model for static light scattering data fitting and were represented by using an EASI graph with a UV peak in the ASTRA V software (Wyatt).

Fluorescent Polarization. Binding affinities of yNta1 (or various yNta1 mutants) and peptides were determined by using fluorescence polarization techniques. Briefly, purified yNta1 proteins were serially diluted in assay buffer at concentrations of 24–400 μM and were mixed into each reaction well. C-terminal FITC-labeled NVK-peptide and QVK-peptide were purchased from Peptron were dissolved in a solution containing 50 mM Tris·HCl pH 8.0, 100 mM NaCl, 1 mM TCEP, and 0.0025% Tween-20, and were adjusted to a concentration of 10 nM for each 25-μL reaction well. Fluorescent measurements were performed in a 96-well plate on a Molecular Device plate reader with excitation and emission wavelengths of 485 and 530 nm, respectively. A nonlinear graph of Nta1 concentration-dependent polarization was drawn and calculated by using GraphPad Prism 5 software.
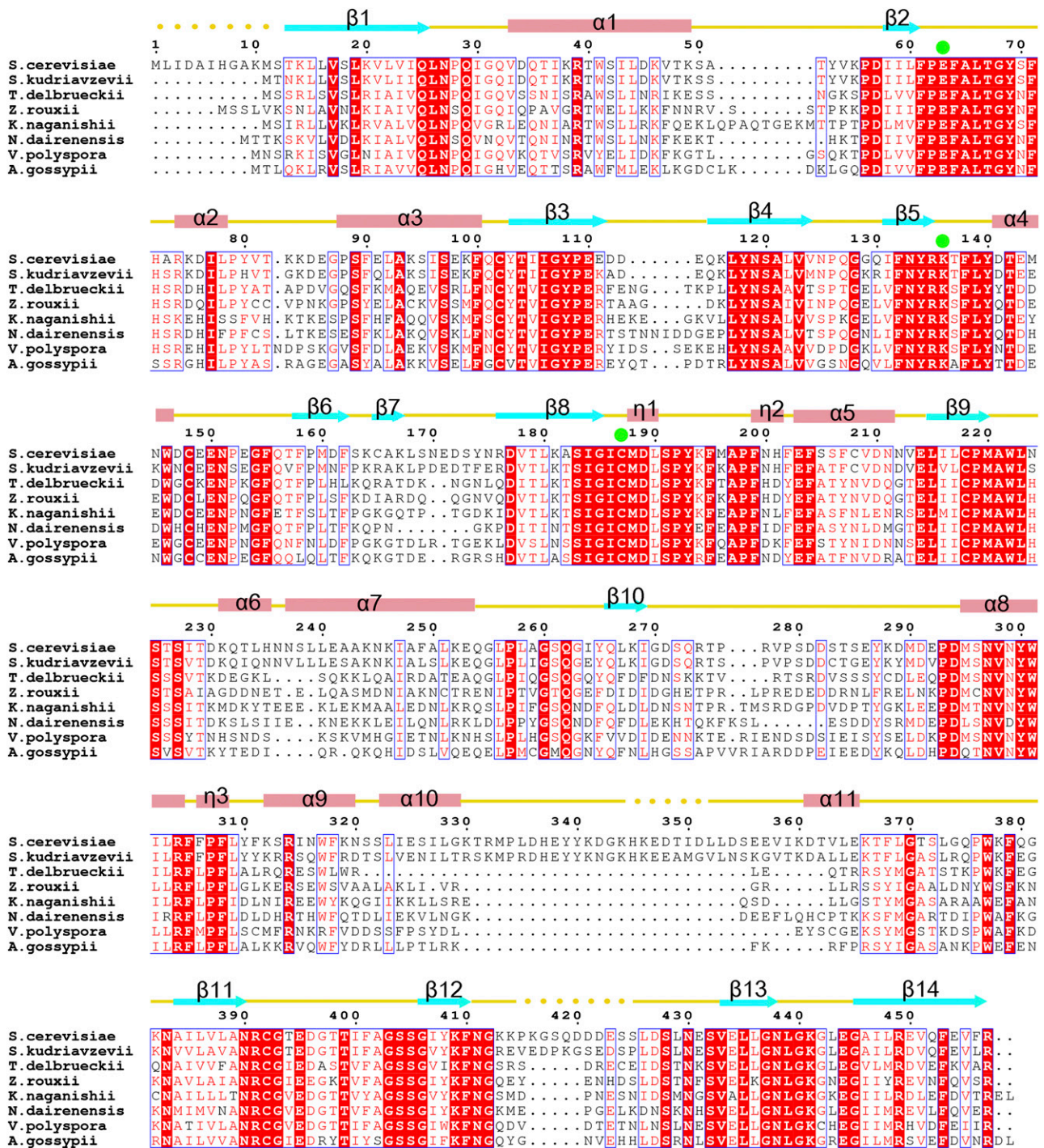
Fig. S1. Sequence alignments of Nta1 sequelogs from *S. cerevisiae, Saccharomyces kudriavzevii, Torulaspora delbrueckii, Zygosaccharomyces rouxii, Kazachstania naganishii, Naumovozyma dairenensis, Vanderwaltozyma polyspora,* and *Ashbya gossypii*. Boxes indicate residues that are identical (red shading) or highly conserved (red font) in all sequences. Secondary structural elements of yNta1 (α-helices, 3₁₀-helices, and β-strands) are shown above sequence alignments, and every 10th residue of Nta1 from *S. cerevisiae* (first row) is marked with a dot and the corresponding residue number. Catalytic residues in the active site are indicated by filled green circles.
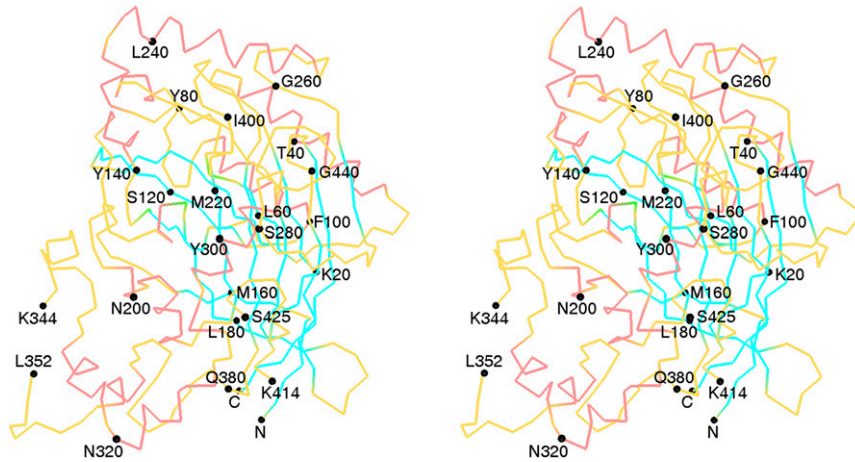
Fig. S2. A stereoview of the Cα trace of yNta1. The orientation and colors are the same as in Fig. 1A. Approximately every 20th residue is marked with a dot and labeled.
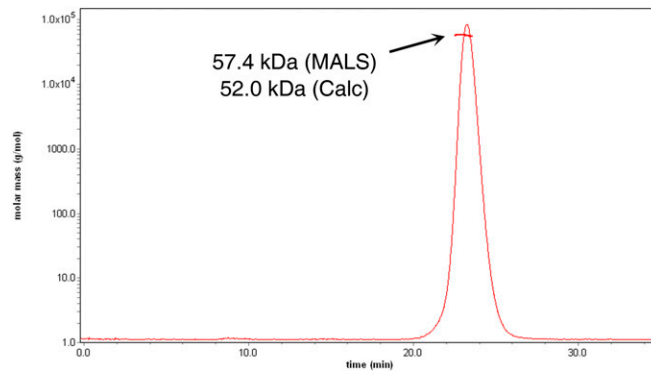

Fig. S3. Oligomeric state of yNta1 in solution. Purified yNta1 was analyzed by using SEC–MALS. The horizontal axis represents the experimentally determined molecular mass (57.4 kDa, MALS), and the theoretically calculated molar mass value is indicated on the vertical axis (52.0 kDa, Calc). yNta1 is clearly present as a monomer in solution.
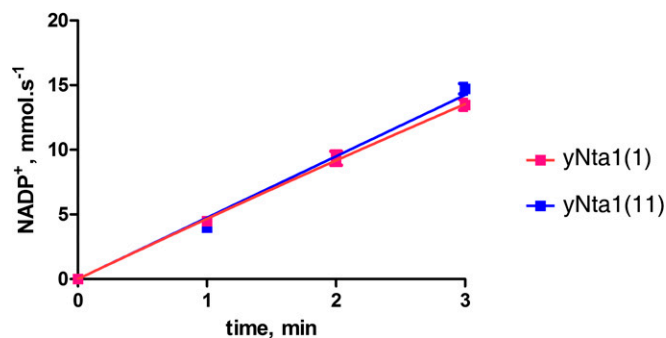

Fig. S4. Comparison of N-terminal deamidase activity between full-length yNta1 and the truncated version yNta11. GLDH-coupled enzyme kinetics of purified wild-type yNta1 (magenta line) and yNta11 (blue line) with 6 mM NV dipeptide substrate. Standard derivations for triplicate measurements are indicated with error bars. No differences in enzyme activity were observed.
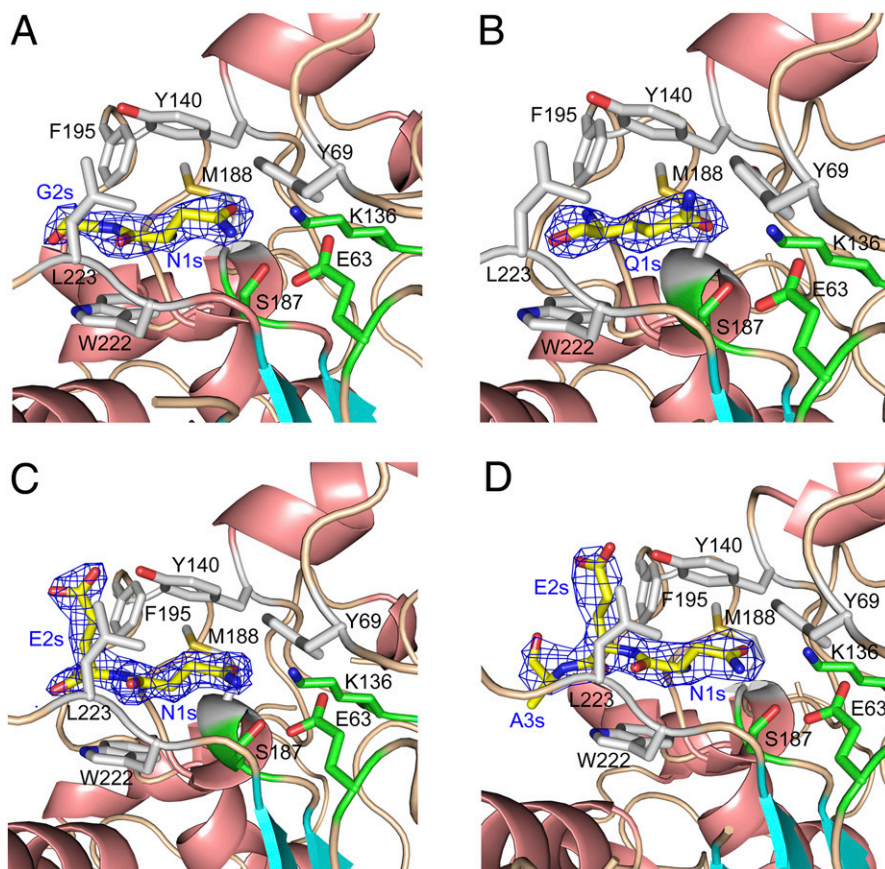
Fig. S5. Close-up view of the N-degron binding site and electron-density maps for the bound N-degron, Asn–Gly (*A*), Gln–Gly (*B*), and Asn–Glu (*C*) dipeptides, and the Asn–Glu–Ala tripeptide (*D*). Side chain atoms of catalytic and interacting residues of yNta1 are shown as green and gray sticks, respectively. N-degron peptides are also shown as yellow sticks. Oxygen and nitrogen atoms are colored red and blue, respectively. N-degron residues are labeled "s" after the residue number for clarity. Electron-density maps were generated and shown as blue mesh for each peptide (*2Fo-Fc* map contoured at 1.0 σ).

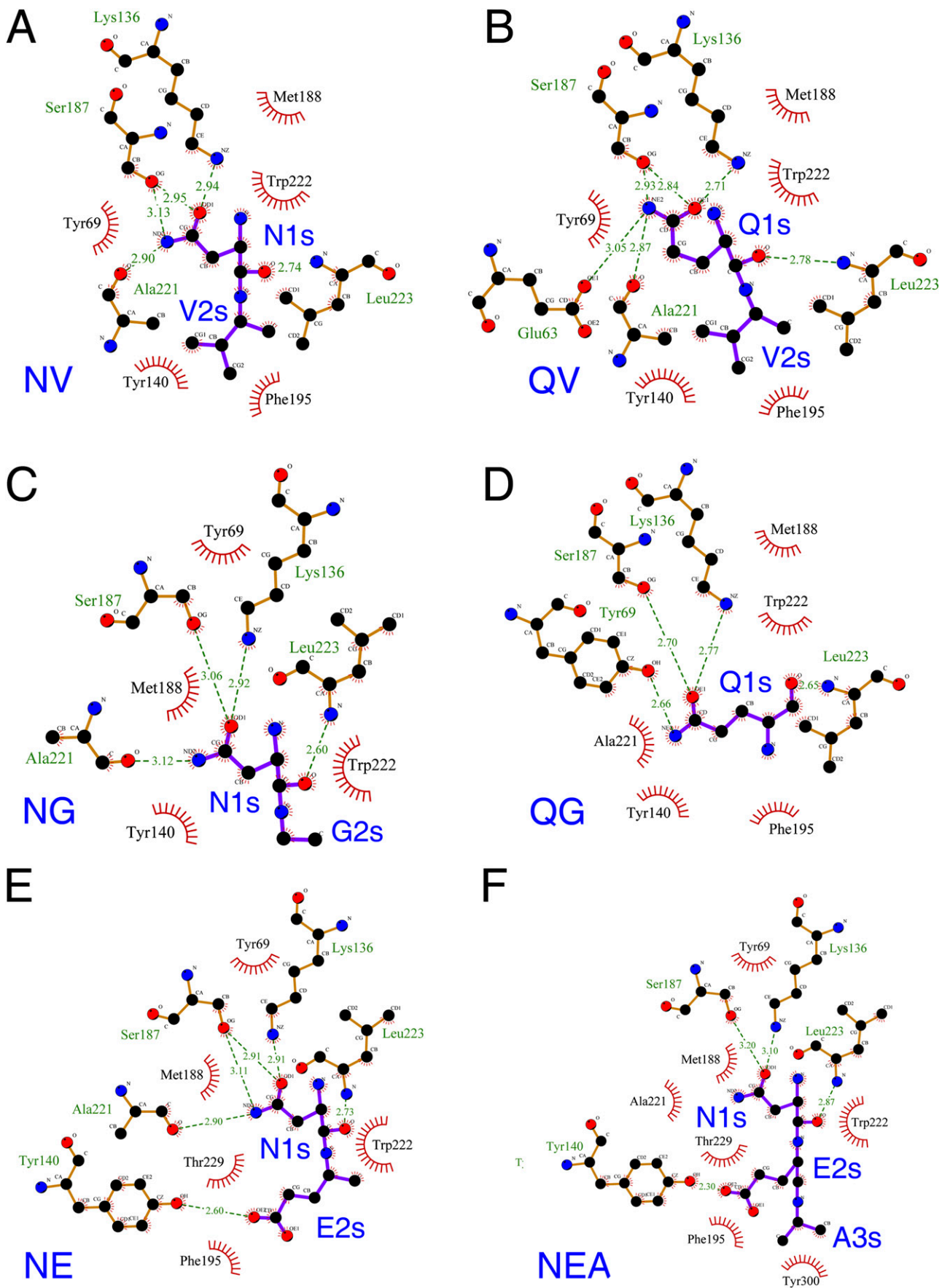**Fig. S6.** Schematic of interactions between yNta1 and N-degron, Asn–Val (*A*), Gln–Val (*B*), Asn–Gly (*C*), Gln–Gly (*D*), Asn–Glu (*E*) dipeptides, and the Asn–Glu–Ala tripeptide (*F*). Hydrophobic interactions are indicated with red starbursts, and hydrogen bonding interactions are shown as green dashed lines with hydrogen bonding distances. N-degron residues are labeled blue for clarity.
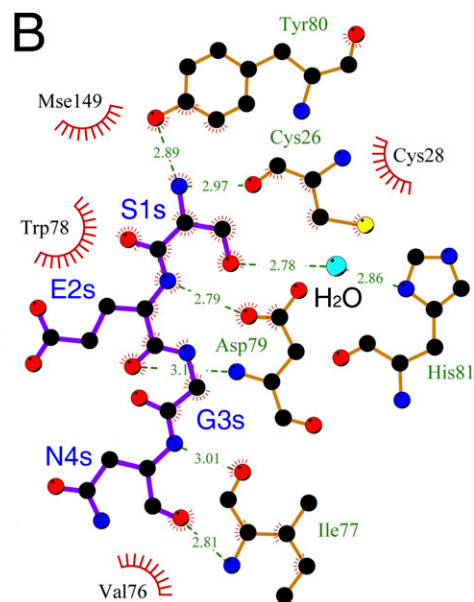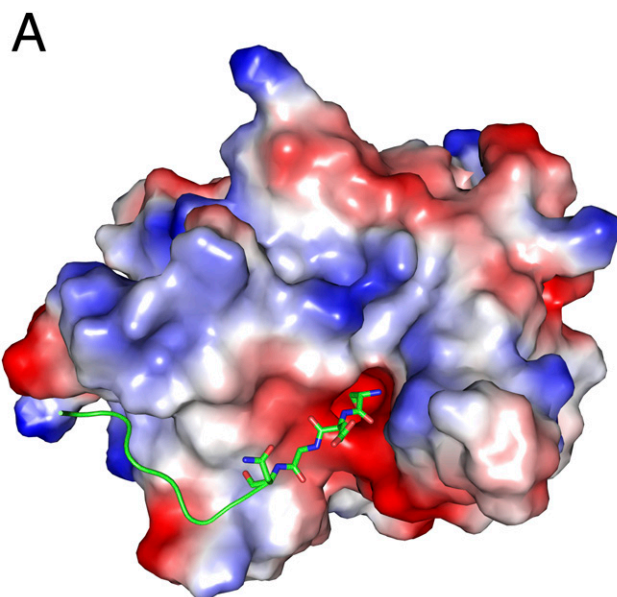
Fig. S7. Structure of human Ntaq1 (PDB ID code 4W79). (*A*) Molecular surface represented by the electrostatic potential surface of hNtaq1 with the N-terminal segment bound to the neighboring molecule in the crystalline lattice. Negatively and positively charged surfaces are indicated in red and blue, respectively. The N-terminal segment is shown as a stick model. (*B*) Schematic of interactions between hNtaq1 and an N-terminal segment that is not an N-end rule substrate. Hydrophobic interactions are denoted by red starbursts and hydrogen bonding interactions are indicated as green dashed lines with hydrogen bonding distances. Residues in the substrate are labeled blue, and the letter "s" is appended to their sequence numbers.
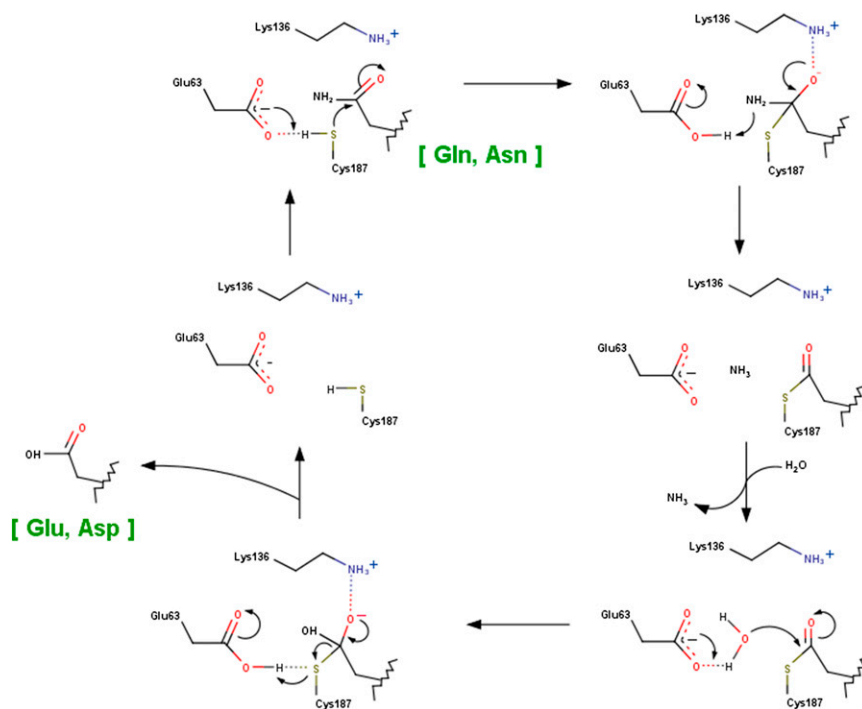

Fig. S8. A schematic diagram showing the proposed mechanism of deamidation reaction catalyzed by yNta1. The carboxyl group of Glu63 enhances the nucleophilicity of Cys187, and the ε-amino group of Lys136 stabilizes the tetrahedral intermediate. A water molecule involves in deacylation step although it is not observed in our crystal structures.

Table S1. Data collection, phasing, and refinement statistics of apo-yNta1

	yNta1 (1)	yNta1 (11)	yNta1 (11) C187S	yNat1 (11) M196L (SeMet)		
				Peak	Edge	Remote
Data collection						
Space group	$P4_2$	$I4_122$	$I4_122$		$I4_122$	
Cell dimensions						
a, b, c, Å	94.9, 94.9, 61.3	133.7, 133.7, 119.2	134.1, 134.1, 119.5		133.0, 133.0, 120.6	
α, β, γ, °	90, 90, 90	90, 90, 90	90, 90, 90		90, 90, 90	
Wavelength	0.97951	1.00000	0.97960	0.97914	0.97929	0.98709
Resolution, Å	50.0–2.32 (2.32–2.36)*	50.0–2.70 (2.70–2.75)	50.0–1.94 (1.94–1.99)	50.0–2.33 (2.33–2.37)	50.0–2.34 (2.34–2.38)	50.0–2.37 (2.37–2.41)
R_{merge}[†]	5.8 (42.1)	6.8 (25.6)	8.3(60.2)	9.4 (48.1)	8.7 (50.1)	8.5 (49.4)
$I/\sigma I$	42.4 (4.18)	63.0 (14.4)	59.5(10.5)	52.8 (6.63)	54.4 (6.6)	53.5 (6.31)
Completeness, %	99.9 (100)	99.9 (100)	99.8 (99.9)	100 (100)	100 (100)	100 (100)
Redundancy	8.1 (8.2)	16.1 (16.4)	16.4 (15.5)	15.2 (15.6)	15.3 (15.9)	15.4 (16.0)
Phasing, no. of Se	—	—	—	—	7	—
Refinement						
Resolution, Å	37.5–2.32	29.9–2.70	38.2–1.94			
No. of reflections	23,487	14,836	39,925			
R_{work}/R_{free}[‡]	0.195/0.242	0.209/0.265	0.178/0.216			
No. of atoms						
Protein	3,318	3,330	3,368			
Water	103	92	371			
B factors, Å^2						
Protein	48.0	42.5	25.4			
Water	45.9	39.3	35.8			
RMSDs						
Bond lengths, Å	0.004	0.002	0.007			
Bond angles, °	0.806	0.632	1.065			
Ramachandran plot						
Favored region, %	97.15	95.97	97.18			
Allowed, %	2.61	3.79	2.59			
Outliners, %	0.24	0.24	0.23			
PDB ID code	5HYY	5K5U	5K5V			

*Values in parentheses are for reflections in the highest resolution bin.

[†]$R_{merge} = \sum_h \sum_i |I(h,i) - \langle I(h) \rangle| / \sum_h \sum_i I(h,i)$, where $I(h,i)$ is the intensity of the ith measurement of h and $\langle I(h) \rangle$ is the corresponding average value for all i measurements.

[‡]R_{work} and $R_{free} = \sum ||F_O| - |F_C|| / \sum |F_O|$ for the working set and test set (5%) of reflections.

Table S2. Data collection and refinement statistics of yNta1 (11) C187S–peptide complex

	NG	NV	NE	QG	QV	NEA
Data collection						
Space group	$I4_122$	$I4_122$	$I4_122$	$I4_122$	$I4_122$	$I4_122$
Cell dimensions						
a, b, c, Å	134.4, 134.4, 119.8	134.6, 134.6, 119.4	134.6, 134.6, 119.1	133.6, 133.6, 119.1	133.8, 133.8, 119.1	133.8, 133.8, 118.9
α, β, γ, °	90, 90, 90	90, 90, 90	90, 90, 90	90, 90, 90	90, 90, 90	90, 90, 90
Wavelength	0.97960	0.97960	0.97960	0.97960	0.97960	0.97960
Resolution, Å	50.0–2.50 (2.50–2.54)*	50.0–1.90 (1.90–1.93)	50.0–2.00 (2.00–2.03)	50.0–2.00 (2.00–2.03)	50.0–1.90 (1.90–1.95)	50.0–3.05 (3.05–3.10)
R_{merge}[†]	7.6 (54.7)	7.1 (53.6)	6.9 (53.1)	5.7 (53.3)	7.3 (51.9)	11.6 (54.6)
$I/\sigma I$	56.3 (8.88)	72.6 (14.5)	70.2 (14.3)	66.0 (6.63)	58.3 (8.67)	32.5 (6.42)
Completeness, %	99.9 (100)	99.6 (100)	99.8 (100)	99.9 (100)	99.9 (100)	99.9 (100)
Redundancy	15.2 (16.2)	16.2 (15.2)	15.2 (16.1)	15.7 (15.7)	16.3 (15.6)	13.2 (13.2)
Refinement						
Resolution, Å	38.2–2.50	29.3–1.90	38.1–2.00	33.4–2.00	38.1–1.90	33.0–3.04
No. of reflections	19,185	43,119	36,928	36,454	42,649	10,652
R_{work}/R_{free}[‡]	0.185/0.246	0.183/0.224	0.174/0.214	0.188/0.214	0.190/0.232	0.205/0.253
No. of atoms						
Protein	3,334	3,296	3,338	3,340	3,326	3,313
Water	86	401	316	243	333	154
Ligand	13	16	18	10	17	26
B factors, Å²						
Protein	47.6	26.2	28.0	35.2	26.5	45.5
Water	47.9	27.0	36.3	41.9	34.9	48.4
Ligand	45.6	37.6	28.5	40.5	32.1	41.6
RMSDs						
Bond lengths, Å	0.005	0.007	0.007	0.007	0.007	0.001
Bond angles, °	0.866	1.032	1.037	1.029	1.029	0.402
Ramachandran plot						
Favored region, %	97.16	98.10	97.39	97.40	97.40	96.41
Allowed, %	2.60	1.66	2.37	2.36	2.36	3.35
Outliners, %	0.24	0.24	0.24	0.24	0.24	0.24
PDB ID code	5K63	5K62	5K66	5K61	5K60	5B62

*Values in parentheses are for reflections in the highest resolution bin.

[†]$R_{merge} = \sum_h \sum_i |I(h,i) - \langle I(h) \rangle| / \sum_h \sum_i I(h,i)$, where $I(h,i)$ is the intensity of the ith measurement of h and $\langle I(h) \rangle$ is the corresponding average value for all i measurements.

[‡]R_{work} and $R_{free} = \sum ||F_O| - |F_C|| / \sum |F_O|$ for the working set and test set (5%) of reflections.